Acta Cryst. (1996). B52, 100–109

Incommensurately Modulated Structure of $TaGe_{0.354}Te_2$: Application of Crenel Functions

F. BOUCHER,[a] M. EVAIN[a] AND V. PETŘÍČEK[b]

[a]*Laboratoire de Chimie des Solides, IMN, UMR CNRS No. 110 – Université de Nantes, 2 rue de la Houssinière, 44072 Nantes CEDEX 03, France, and* [b]*Institute of Physics, Academy of Sciences of the Czech Republic, Na Slovance 2, 180 40 Praha 8, Czech Republic*

(*Received 4 May 1995; accepted 26 July 1995*)

Abstract

The incommensurately modulated structure of tantalum germanium telluride, $TaGe_{0.354}Te_2$, was determined by single-crystal X-ray diffraction. The dimensions of the basic orthorhombic cell are $a = 6.4394(5)$, $b = 14.025(2)$, $c = 3.8456(5)$ Å, $V = 347.3(1)$ Å^3 and $Z = 4$. The $(3 + 1)$-dimensional superspace group is $Pnma(00\gamma)s00$, $\gamma = 0.3544(3)$. Refinements on 1641 reflections with $I \geq 3\sigma(I)$ converged to $R = 0.065$ and 0.044 for 526 main reflections and $R = 0.061$, 0.12, 0.28 and 0.32 for 782 first-order, 237 second-order, 37 third-order and 59 fourth-order satellites, respectively. Since the structure exhibits a strong occupational modulation of both Ta and Ge atoms, along with important displacive modulation waves, crenel functions were used in the refinement in combination with an orthogonalization procedure. Such an approach is shown to be the most convenient and to give reliable coordinations and distances. A detailed analysis of some Te···Te distances is performed, in connection with already known commensurately and incommensurately modulated MA_xTe_2 structures.

1. Introduction

In most solid-state chemistry publications, a great deal of attention is paid to the cationic species and the anions are only considered in terms of polyhedra coordinating those cationic species. However, the anions cannot be entirely ignored or just considered as a framework contributing to electronic bands well below or well above the Fermi level. In fact, recent studies have clearly shown the crucial part of the formation of anionic entities (either as small groups or as extended arrays) in, for instance, the stability of the phases or the physical properties (Jobic, Brec & Rouxel, 1992; Rouxel, 1993). This part is particularly evident in tellurides (Böttcher, 1988; Mar, Jobic & Ibers, 1992; Canadell, Jobic, Brec, Rouxel & Whangbo, 1992; Canadell, Monconduit, Evain, Brec, Rouxel & Whangbo, 1993). By virtue of its high *sp* levels, *i.e.* its low electronegativity, and the diffuse character of its orbitals, tellurium is indeed prone to compete with metals. Certainly, the overlap between the *sp* anionic levels and the *d* cationic ones can result in an electron transfer from the top of the *sp* band towards the *d* band. The extra electrons on the metals can be used in the formation of metal–metal bonds. Also, the holes on the anionic band can result in the formation of short Te···Te bonding contacts. It has been shown (Canadell *et al.*, 1992; Canadell *et al.*, 1993) that the latter structural response is more likely to occur in layered materials with the development of short interslab contacts involving the tellurium p_z orbital (perpendicular to the layer).

The quest for new evidence of these electronic competitions and charge transfers led us to investigate the *M*–*A*–Te (*M* = Nb; Ta; *A* = Si, Ge) phase diagram. A new family was found with the homologous MA_xTe_2 (*M* = Nb, Ta; *A* = Si, Ge; $\frac{1}{3} \leq x \leq \frac{1}{2}$) series (Monconduit, Evain, Boucher, Brec & Rouxel, 1992; Li & Caroll, 1992; Li, Badding & DiSalvo, 1992; Monconduit, Evain, Brec, Rouxel & Canadell, 1993; Evain, Monconduit, van der Lee, Brec, Rouxel & Canadell, 1994; Evain, van der Lee, Monconduit & Petříček, 1994; van de Lee, Evain, Mansuetto, Monconduit, Brec & Rouxel, 1994; van der Lee, Evain, Monconduit, Brec & van Smaalen, 1994; van der Lee, Evain, Monconduit, Brec, Rouxel & Petříček, 1994; van der Lee & Evain, 1995; Gareh, Boucher & Evain, 1995; Evain, Monconduit & van der Lee, 1995). The MA_xTe_2 structures are not simply derived from that of MTe_2, since *M* is in a trigonal prismatic rather than in the usual octahedral Te environment. In addition, the *A* atoms adopt a very unusual square-planar coordination in the common face of two trigonal Te prisms. For most MA_xTe_2 phases, *i.e.* those with $x \neq \frac{1}{2}$, the charge balance is not straightforward, thus implying a charge transfer from the Te p_z band to the *M d* band (Canadell *et al.*, 1993; Evain, Monconduit, van der Lee, Brec, Rouxel & Canadell, 1994). In addition, short Te···Te interslab distances were calculated for all phases. However, it was recently clearly demonstrated (Evain, Monconduit & Brec, 1995) that these short contacts do exist in all the MA_xTe_2 phases, with or without charge transfer, due to steric effects.

The MA_xTe_2 structures are characterized by a strong occupational modulation of both M and A, along with important displacive modulation waves of all the atoms. Precise structure determinations, pertinent for bond length and geometry characterization and consequently for electronic considerations, could be easily achieved for the commensurate MA_xTe_2 phases (x rational). They were not so conclusive for the incommensurately modulated phases (x irrational), often yielding large ranges of distances, because of the very nature of the harmonic functions usually chosen to model both the occupational and the displacive modulations. The use of a crenel function should, in principal, get round these drawbacks. However, it should be combined with an orthogonalization procedure and an eventual selection of the basic functions, as has been shown recently (Petříček, van der Lee & Evain, 1995).

In this paper we report the structure determination of a new incommensurately modulated phase, $TaGe_{0.354}Te_2$. We will discuss the use of crenel functions and show that it allows the establishment of 'true' interatomic distances, thereby allowing discussion of short Te···Te contacts and charge transfer.

2. Experimental

2.1. *Synthesis*

$TaGe_{0.354}Te_2$ was obtained in an attempt to prepare $TaGe_{3/7}Te_2$ by direct combination of the elements in stoichiometric proportion. The mixture was placed under vacuum in a sealed silica tube and heated at 1223 K for a 10 d period. Subsequent cooling to room temperature was achieved at a speed of 100 K h^{-1}. Many platelets with a metallic luster were found in the batch. A semi-quantitative analysis with a scanning electronic microscope yielded the formulation $Ta_{0.9}Ge_{0.3}Te_2$.

2.2. *Data collection*

A single crystal of sufficient quality was selected and tested with the usual rotation and Weissenberg techniques. Considering the main reflections only, a primitive orthorhombic lattice ($a \simeq 6.4$, $b \simeq 14.0$ and $c \simeq 3.8$ Å) close to that of other MA_xTe_2 compounds was found. In addition, a sublattice of weaker spots could be identified corresponding to an almost threefold superstructure along the c axis. From a careful analysis of the films, it was deduced that the superstructure is incommensurate with the main lattice. The crystal was then mounted on a Siemens P4 diffractometer to precisely determine the lattice metric. An accurate centering of 67 *hkl* (28 main and 39 first-order reflections) followed by a 2θ least-squares refinement with the *U-FIT* program (Evain, 1992) gave the following cell parameters: $a = 6.4394(5)$, $b = 14.025(2)$, $c = 3.8456(5)$ Å and $\mathbf{q} = 0.3544(3) \times \mathbf{c}^*$.

Table 1. *Experimental details*

Crystal data	
Chemical formula	$TaGe_{0.354}Te_2$
Chemical formula weight	461.9
Cell setting	Orthorhombic
Superspace group	$Pnma(000\text{-}\gamma)s00$
a (Å)	6.4394 (5)
b (Å)	14.025 (2)
c (Å)	3.8456 (5)
V (Å^3)	347.3 (1)
Z	4
Modulation vector	$\mathbf{q} = 0.3544\ (3)\ \mathbf{c}^*$
$F(000)$	753
D_x (g cm^{-3})	8.83
Radiation type	Mo $K\alpha$
Wavelength (Å)	0.71073
No. of reflections for cell parameters	67
θ range (°)	7.5–28.4
μ (mm^{-1})	50.84
Temperature (K)	293
Crystal form	Platelet
Crystal size (mm^3)	8.6×10^{-4}
Crystal color	Black
Data collection	
Diffractometer	Enraf–Nonius CAD-4F
Monochromator	Oriented graphite (002)
Data collection method	ω/θ
Absorption correction	Gaussian integration
T_{min}	0.08
T_{max}	0.77
No. of measured reflections	9971
No. of independent reflections	4744
No. of observed reflections	1660
Criterion for observed reflections	$I \geq 3\sigma(I)$
R_{int}	0.044
θ_{max} (°)	35
Range of h, k, l	$-1 \rightarrow h \rightarrow 10$ $-1 \rightarrow k \rightarrow 22$ $-6 \rightarrow l \rightarrow 6$
No. of standard reflections	19
Frequency of standard reflections	Every 60 min
Intensity decay (%)	5.3
Refinement	
Refinement on	F
R	0.064
$wR(F^2)$	0.062
S	2.25
No. of reflections used in refinement	1641
No. of parameters used	69
Weighting scheme	$w = 1/[\sigma^2(\lvert F_o\rvert) + (0.01F_o)^2]$
$(\Delta/\sigma)_{max}$	0.2
$\Delta\rho_{max}$ (e Å^{-3})	7.9
$\Delta\rho_{min}$ (e Å^{-3})	−10.6
Extinction method	Isotropic extinction – type I
Extinction coefficient	1.7×10^{-6}
Source of atomic scattering factors	*International Tables for X-ray Crystallography* (1974, Vol. IV)
Computer programs	
Data collection	*CAD-4 Software* (Enraf–Nonius, 1989)
Cell refinement	*U-FIT* (Evain, 1992)
Data reduction	*Xtal*3.2 (Hall, Flack & Stewart, 1992)
Structure refinement	*JANA*94 (Petříček, 1995)

The data collection was performed on an Enraf–Nonius CAD-4F diffractometer with monochromatized Mo K-$L_{2,3}$ radiation, using an ω/θ technique. In relation

Table 2. *Reflection statistics*

	N_1	N_2	$\langle I \rangle$	$\langle I/\sigma(I) \rangle$
Main	2240	1147	100.0	19.01
First-order	2671	1230	54.6	15.73
Second-order	1566	398	14.4	7.75
Third-order	1486	44	6.9	4.90
Fourth-order	1509	70	6.1	4.63
All	9472	2889	65.2	15.49

N_1 is the total number of data collected, N_2 is the number of data with $I/\sigma(I) \geq 3.0$, $\langle I \rangle$ and $\langle I/\sigma(I) \rangle$ are calculated for the N_2 data. The values in the column for $\langle I \rangle$ are normalized to 100.0 for the strongest reflection class. The internal R factor for averaging in the *mmm* Laue class is 4.4%. 1660 unique reflections are left for refinement.

to the modulation wavelength ($\sim \frac{1}{3}\mathbf{c}^*$), many reflections are overlapping in a bisecting mode. A first data collection in such a mode led to unsatisfactory results. A nonzero PSI mode (azimuth) was then considered. Since for the four-circle geometry the best angular resolution is in the horizontal plane, $\mathbf{c}^*$ had to be brought as close as possible to that plane. Therefore, for each reflection the PSI angle was chosen to ensure both a good separation of the reflections and a minimization of the absorption effect. Considering the value of the linear absorption coefficient ($\mu = 508\,\text{cm}^{-1}$), the minimum acceptable glancing angle was taken as 15°. 2258 subcell reflections in the ranges $-1 \leq h \leq 10$, $-1 \leq k \leq 22$ and $-6 \leq l \leq 6$ were measured and in a second run 7713 satellite reflections up to the fourth order in the ranges $-1 \leq h \leq 10$, $-1 \leq k \leq 22$ and $-1 \leq l \leq 6$. In the course of the data reduction, reflections with either an asymmetric background (BG left/BG right $\notin$ [1/3,3]) or a deviated position were rejected. 9472 *hkl* reflections were then kept for further processing. Recording conditions and reflection statistics are gathered in Tables 1 and 2, respectively.

2.3. *Data processing*

The measured intensities were corrected for scale variation and Lorentz and polarization effects. A Gaussian-type absorption correction was then applied with the *Xtal*3.2 system (Hall, Flack & Stewart, 1992). Since this system does not handle real indices, a supercell approach ($c' = 31 \times c$) was used. Given the lack of accuracy on the measurement of the platelet thickness, an optimization of the crystal dimensions was initiated. A final thickness of 0.0050 mm was found to give the best results for both the averaging internal factor for the main reflections and the refinement reliability factors. The Laue symmetry proved to be *mmm* and the intensities were therefore averaged accordingly ($R_{\text{int}} = 4.4\%$). A final set of 1660 independent reflections with $I > 3\sigma(I)$ was left for refinement. At the final stage (*vide infra*), 19 reflections had to be skipped due to large $\Delta(F_{\text{calc}} - F_{\text{obs}})$, probably in relation to a not completely solved overlapping problem.

2.4 *Structure refinement*

The systematic extinctions are: $k + l + m = 2n + 1$ and $h = 2n + 1$ for the $(0klm)$ and $(hk00)$ reflections, respectively. They indicate the presence of two different glide planes: $\{m_x 1 | 0 \frac{1}{2} \frac{1}{2} \frac{1}{2}\}$ and $\{m_z \bar{1} | \frac{1}{2} 000\}$. The only possible centrosymmetric space group is $Pnma(00\gamma)s00$. This superspace group was also found for the other incommensurately modulated compounds of the MA_xTe_2 family, *i.e.* $TaSi_{0.360}Te_2$ (van der Lee, Evain, Monconduit, Brec, Rouxel & Petříček, 1994) and $TaSi_{0.414}Te_2$ (Evain, van der Lee *et al.*, 1994), and for some commensurately modulated compounds, such as $NbGe_{3/7}Te_2$ (van der Lee, Evain, Monconduit, Brec & van Smaalen, 1994). It is equivalent to the conventional superspace group $Pnma(00\gamma)$ from *International Tables for Crystallography* (1992, Vol. C) by the choice of the equivalent wavevector $\mathbf{q} = \mathbf{q} - \mathbf{c}^*$. Our choice ($\mathbf{q} = 0.3544\mathbf{c}^*$) allows us to assign the strongest satellites to the first-order $m = 1$ (van der Lee, Evain, Monconduit, Brec & van Smaalen, 1994), which makes the indexing more transparent.

The nonlinear least-squares refinements were performed with the *JANA*94 program system (Petříček, 1994). The scattering factors for neutral atoms and the anomalous dispersion correction parameters were taken from *International Tables for X-ray Crystallography* (1974, Vol. IV). All refinements were based on F_{obs} and performed in a full-matrix mode, using $w = 1/[\sigma^2(|F_{\text{obs}}|) + (0.01F_{\text{obs}})^2]$ as weights.

First, the refinements were performed with the main reflections only, *i.e.* without any modulation parameters. Good initial atomic positions were obtained from previous MA_xTe_2 structural determinations, that is to say three atoms [Ta(1), Ta(2) and Ge] on the m_y mirror plane and one Te atom on a general position (see Fig. 1 and Table 3). With isotropic atomic displacement parameters (ADPs) and the refinement of Ta and Ge occupation ratios, the reliability factors converged to $R = 0.237$, $wR = 0.258$. As expected from simple structural considerations (van der Lee, Evain, Monconduit, Brec & van Smaalen, 1994), the sum of the occupation probabilities of Ta(1) and Ta(2) reached a value close to 1.0 and the occupation probability of Ta(2) and Ge took the $\gamma = 0.3544$ value, within a 3σ error level. Accordingly, in the subsequent refinements the occupation probabilities of Ta(1), Ta(2) and Ge atoms were fixed to 0.6456, 0.3544 and 0.3544, respectively.

From our knowledge of the MA_xTe_2 structure characteristics, especially that of the commensurate cases, strong modulations were expected for both the cation occupation probabilities and the anion positions. Modulations of positions were expressed as a three-dimensional Fourier sum of a limited number of harmonics

$$\mathbf{r}^{\nu}(x_4) = \mathbf{r}_0^{\nu} + \sum_n [\mathbf{u}_{s,n}^{\nu} \sin(2\pi n x_4) + \mathbf{u}_{c,n}^{\nu} \cos(2\pi n x_4)],$$

Table 3. *Final values for the amplitudes of the displacive modulation functions*

	n	$A^{\nu}_{xs,n}$	$A^{\nu}_{ys,n}$	$A^{\nu}_{zs,n}$	$A^{\nu}_{xc,n}$	$A^{\nu}_{yc,n}$	$A^{\nu}_{zc,n}$
Ta(1)	0				0.3150 (2)	1/4	−0.0489 (4)
					0.3155	1/4	−0.0675
	1	−0.0068 (3)	0	−0.0316 (4)	−0.0065 (2)	0	−0.0423 (3)
		−0.0047	0	−0.0579	−0.0105	0	−0.0500
	2	0.0002 (5)	0	0.0025 (5)	−0.0009 (6)	0	0.0083 (9)
		−0.0009	0	0.0163	−0.0022	0	0.0192
Ta(2)	0				0.0349 (2)	1/4	−0.0566 (7)
					0.0392	1/4	−0.0531
	1	−0.003 (5)	0	0.0169 (8)	0.0009 (6)	0	0.012 (1)
		−0.005	0	0.0114	0.0026	0	0.0346
Ge	0				0.4255 (7)	1/4	0.270 (2)
					0.4252	1/4	0.2284
	1	0.002 (1)	0	0.028 (2)	0.000 (2)	0	−0.005 (2)
		0.003	0	0.065	0.001	0	−0.026
Te(1)	0				0.1424 (2)	0.1171 (1)	0.4910 (4)
					0.1440	0.1164	0.4986
	1	0.0012 (3)	0.0019 (2)	0.0242 (5)	0.0026 (3)	−0.0011 (2)	−0.0204 (4)
		0.0038	0.0007	0.0355	0.0019	−0.0026	−0.0272
	2	−0.0016 (6)	−0.0002 (3)	0.0014 (9)	−0.0018 (7)	0.0004 (4)	−0.004 (1)
		−0.0025	−0.0010	0.0079	−0.0034	0.0008	−0.008
Te(2)	0				0.2118 (3)	0.1158 (1)	0.4805 (6)
					0.2193	0.1178	0.4780
	1	0.0012 (6)	−0.0002 (3)	−0.0120 (8)	−0.0022 (7)	−0.0004 (4)	0.005 (1)
		−0.0056	−0.0020	−0.0111	−0.0082	−0.0014	0.021

The first line for each order of each atom gives the orthogonalized Fourier amplitudes $\mathbf{u}^{\nu,\mathrm{ort}}_{s,n}$ and $\mathbf{u}^{\nu,\mathrm{ort}}_{c,n}$ that result from the refinement; the second line gives the corresponding nonorthogonalized amplitudes.

where ν represents the independent atoms in the basic unit cell, x_4 is the argument of the modulation function: $x_4 = t + \mathbf{q}\cdot\mathbf{r}^{\nu}_{0,L} = t + \mathbf{q}\cdot(\mathbf{r}^{\nu}_{\mathbf{0}} + \mathbf{L})$, with t the global phase of the modulation wave, $\mathbf{r}^{\nu}_{0}$ the average position within the basic unit cell, $\mathbf{L}$ a basic structure lattice translation and where $\mathbf{u}^{\nu}_{s,n} = (A^{\nu}_{xs,n}, A^{\nu}_{ys,n}, A^{\nu}_{zs,n})$ and $\mathbf{u}^{\nu}_{c,n} = (A^{\nu}_{xc,n}, A^{\nu}_{yc,n}, A^{\nu}_{zc,n})$ are the modulation amplitudes.

Fourier series have not been used to describe the cation occupation modulation. In fact, in the case of strong modulations such development requires an important number of harmonics. Furthermore, it has already been shown that for the MA_xTe_2 series, the occupancy modulation is best modeled by a crenel function (van der Lee, Evain, Monconduit, Brec, Rouxel & Petříček, 1994). Such a function can be formally defined as the difference between two Heaviside functions of amplitude 1. The evolution of the occupation ratio P *versus* x_4 is then

$$P^{\nu}(x_4) = 1 \quad \text{for} \quad x_4 \in [x^{\nu}_{4,0} - \tfrac{1}{2}\Delta^{\nu}, x^{\nu}_{4,0} + \tfrac{1}{2}\Delta^{\nu}] \mod 1$$
$$P^{\nu}(x_4) = 0 \quad \text{for} \quad x_4 \notin [x^{\nu}_{4,0} - \tfrac{1}{2}\Delta^{\nu}, x^{\nu}_{4,0} + \tfrac{1}{2}\Delta^{\nu}] \mod 1,$$

where ν represents the independent atoms in the basic unit cell, $x^{\nu}_{4,0}$ is the midpoint of the nonzero interval and Δ^{ν} the width of this interval. This last parameter is just equal to the average occupation probability P^{ν}_{0}.

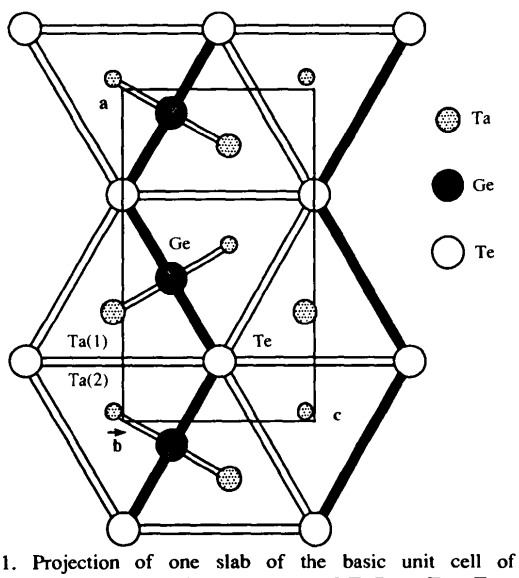

Fig. 1. Projection of one slab of the basic unit cell of the incommensurately modulated structure of $TaGe_{0.354}Te_2$. Te atoms form a hexagonal network; Ta-atom pairs and Ge atoms occupy biprism common faces. The radius of the circles representing Ta atoms is proportional to the occupation probability.

All sets of reflections were taken into account for the refinement of the modulated structure. The first least-squares cycle series was used to find the two first-order Fourier components of the Te displacive modulation and the cation occupation modulation parameters. The Δ^{ν} crenel widths of Ta(1), Ta(2) and Ge were fixed to 0.6456, 0.3544 and 0.3544, respectively (*vide supra*). The $x^{\nu}_{4,0}$ crenel centers were deduced from two series of observations:

(i) The cationic site occupancies should never lead to unrealistic short distances throughout the entire structure. Three mathematical restrictions are necessary to fulfill this requirement. From Fig. 1 it can be seen that whenever the Ta(1) site is occupied, the nearest Ta(2) and Ge sites should be empty. That is, there should be no overlap between the Ta(2) (x_1, x_2, x_3, x_4) or Ge crenel functions and that of Ta(1) (x_1, x_2, x_3, x_4). This implies

the three following relations (of which two are independent

$$x_{4,0}^{\mathrm{Ta(2)}} - \gamma x_3^{\mathrm{Ta(2)}} = x_{4,0}^{\mathrm{Ta(1)}} - \gamma x_3^{\mathrm{Ta(1)}} - \tfrac{1}{2} \quad (1)$$

$$x_{4,0}^{\mathrm{Ge}} - \gamma x_3^{\mathrm{Ge}} = x_{4,0}^{\mathrm{Ta(1)}} - \gamma x_3^{\mathrm{Ta(1)}} - \tfrac{1}{2} \quad (2)$$

$$x_{4,0}^{\mathrm{Ta(2)}} - \gamma x_3^{\mathrm{Ta(2)}} = x_{4,0}^{\mathrm{Ge}} - \gamma x_3^{\mathrm{Ge}}. \quad (3)$$

It is also clear that whenever the Ge site is occupied, the neighboring tantalum sites should be vacant. That is, the Ge (x_1, x_2, x_3, x_4) and Ta(2) $(\frac{1}{2} + x_1, x_2, \frac{1}{2} - x_3, \frac{1}{2} - x_4)$ crenel functions should not extend over one another. An inequality can then be deduced from (3)

$$\tfrac{1}{4}(1 + \gamma) \leq x_{4,0}^{\mathrm{Ta(2)}} - \gamma x_3^{\mathrm{Ta(2)}} \leq \tfrac{3}{4}(1 - \gamma). \quad (4)$$

(ii) The filling of the Ta(2) $(\frac{1}{2} + x_1, x_2, \frac{1}{2} - x_3, \frac{1}{2} - x_4)$ site means the presence of a Ta(1)—Ta(2) pair. This pair is incompatible with the presence of another Ta(1) atom at $(x_1, x_2, 1 + x_3, x_4)$. Therefore, from equation (1) and the fact that the crenel functions of Ta(2) $(\frac{1}{2} + x_1, x_2, \frac{1}{2} - x_3, \frac{1}{2} - x_4)$ and Ta(1) $(x_1, x_2, 1 + x_3, x_4)$ should not overlap, one can deduce the following relation

$$x_{4,0}^{\mathrm{Ta(2)}} - \gamma x_3^{\mathrm{Ta(2)}} = \tfrac{1}{4}(1 + \gamma). \quad (5)$$

It can be easily shown that relation (4) is verified when (5) is fulfilled.

In summary, we have the three following restrictions

$$x_{4,0}^{\mathrm{Ta(1)}} = \tfrac{1}{4}(3 + \gamma) - \gamma x_3^{\mathrm{Ta(1)}}$$
$$x_{4,0}^{\mathrm{Ta(2)}} = \tfrac{1}{4}(1 + \gamma) - \gamma x_3^{\mathrm{Ta(2)}}$$
$$x_{4,0}^{\mathrm{Ge}} = \tfrac{1}{4}(1 + \gamma) - \gamma x_3^{\mathrm{Ge}}.$$

The refinement with isotropic ADPs for all atoms lowered the R/wR factors for the main reflections to 0.171/0.188 (0.282/0.302 for all reflections). New displacive modulations were then introduced: up to second-order for the Fourier components of Ta(1), up to first-order for the Fourier components of Ta(2) and Ge, and to fourth-order for the Fourier components of Te. Isotropic ADPs were converted to anisotropic ones for Ta(1), Ta(2) and Te and an isotropic secondary extinction parameter was introduced. At this refinement level, the final agreement factors for this model were R/wR = 0.054/0.055, 0.068/0.068, 0.149/0.195, 0.329/0.365, 0.368/0.458 and 0.076/0.081 for main, first-order, second-order, third-order, fourth-order and all reflections, respectively.

Although this model gave acceptable R values, it was plainly not stable due to high correlation coefficients between various cationic displacive parameters (13 correlation coefficients were larger than 0.95 in absolute value). This is typical of the use of crenel functions for occupation probability modulations (Petříček *et al.*, 1995). Indeed, since these modulation functions are not defined for all x_4 values, the orthogonality condition is not fulfilled for the set of harmonic functions. With a method based on the Schmidt orthogonalization procedure, it is possible to construct a new orthogonal base from a nonorthogonal set of linearly independent functions (see Petříček *et al.*, 1995, for details). Such an orthogonalization procedure was used in the present case for the cationic displacive modulation functions. Although no significant changes were observed on the R values, the refinement converged more smoothly (the highest correlation coefficient was 0.84 in absolute value).

At this stage, a difference Fourier synthesis revealed electronic density residues around the tellurium position. One can see on the (x_1, x_4) plane (Fig. 2) that the tellurium displacive modulation is not well described by a fourth-order Fourier series expansion. A Fourier map in the same plane (Fig. 3) clearly shows that the displacive modulation of the Te x_1 coordinate has a step-like shape. This is in agreement with the evolution observed for one group of Te—Te distances (within and parallel to the MA_xTe_2 slab) in $TaSi_{0.414}Te_2$ (Evain, van der Lee *et al.*, 1994). Indeed, three different situations were found: (i) Te—Te short contacts above and below the Ta—Ta pairs: d_{avg} = 3.33 Å, (ii) Te—Te long distances above and below the Si atoms: d_{avg} = 3.92 Å and (iii) Te—Te intermediate distances between two prisms of the $[TaTe_2]$-like ribbons: d_{avg} = 3.51 Å. These three

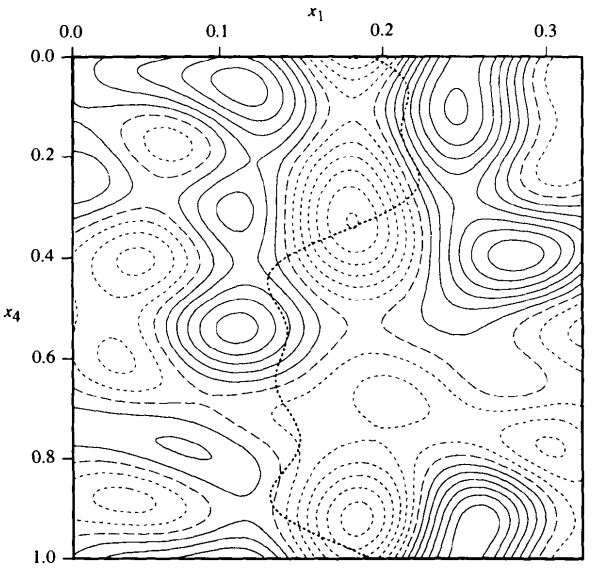

Fig. 2. (x_1, x_4) section of the four-dimensional difference Fourier map around the tellurium position before its splitting. Contour lines from −6 to 6 e Å^{-3} in intervals of 1 e Å^{-3} (positive and negative values in solid and broken lines, respectively). The Te displacive modulation wave is shown as a broken line.

situations are characteristic of all commensurate MA_xTe_2 phases with $x < \frac{1}{2}$ (for $x = \frac{1}{2}$ the intermediate distance is absent).

Thus, to improve the model the tellurium position was split into two positions, Te(1) at low x_1 values ($x_1 \simeq 0.14$) and Te(2) at high x_1 values ($x_1 \simeq 0.21$), with their own occupation crenel functions. However, these functions are not independent and, in addition, should be related to the cation crenel functions. The tellurium Δ^ν and $x^\nu_{4,0}$ parameter restrictions were deduced from the following considerations:

(i) The Te(2) position should be limited to the t range corresponding to the presence of a Ta(1)—Ta(2) pair (see Fig. 1). This requirement is fulfilled if there is a perfect matching of the crenel functions of Te(2) (x_1, x_2, x_3, x_4) and Ta(2) $(\frac{1}{2}+x_1, x_2, \frac{1}{2}-x_3, \frac{1}{2}-x_4)$, *i.e.* when

$$\Delta^{\mathrm{Te(2)}} = 0.3544, \quad \text{and}$$
$$x^{\mathrm{Te(2)}}_{4,0} = \tfrac{1}{4}(1-3\gamma) + \gamma x_3^{\mathrm{Te(2)}}.$$

(ii) There should be no overlap between the Te(1) and Te(2) crenel functions, which corresponds to the following restrictions

$$\Delta^{\mathrm{Te(1)}} = 0.6456, \quad \text{and}$$
$$x^{\mathrm{Te(1)}}_{4,0} = \tfrac{3}{4}(1-\gamma) + \gamma x_3^{\mathrm{Te(1)}}.$$

Apart from those restrictions, the two tellurium positions were refined independently, with anisotropic ADPs for both atoms and displacive modulations up to second-order for Te(1) and first-order for Te(2).

Table 4. *Final reliability factors for* $TaGe_{0.354}Te_2$

	N	R	wR
Main	526	0.0443	0.0440
First-order	782	0.0610	0.0552
Second-order	237	0.120	0.139
Third-order	37	0.277	0.305
Fourth-order	59	0.325	0.412
Overall	1641	0.0645	0.0623

N is the number of data used in the refinement (for 69 parameters).

Moreover, an orthogonalization procedure was used for both positions. This procedure gave the following reliability factors: $R/wR = 0.049/0.050$, 0.066/0.065, 0.137/0.186, 0.28/0.319, 0.321/0.42 and 0.070/0.076 for main, first-order, second-order, third-order, fourth-order and all reflections, respectively. After suppressing the 19 worst reflections ($w^{1/2}|F_{\mathrm{obs}} - F_{\mathrm{calc}}| > 10$), the final R values converged to: $R/wR = 0.044/0.044$, 0.061/0.055, 0.12/0.139, 0.277/0.305, 0.325/0.412 and 0.064/0.062 for main, first-order, second-order, third-order, fourth-order and all reflections, respectively. No significant electronic density residues were then found around the tellurium positions (see Fig. 4). The results of the final refinement have been compiled in Tables 3, 4 and 5.*

* The orthogonalized function set and lists of observed and calculated structure factors have been deposited with the IUCr (Reference: DU0402). Copies may be obtained through The Managing Editor, International Union of Crystallography, 5 Abbey Square, Chester CH1 2HU, England.

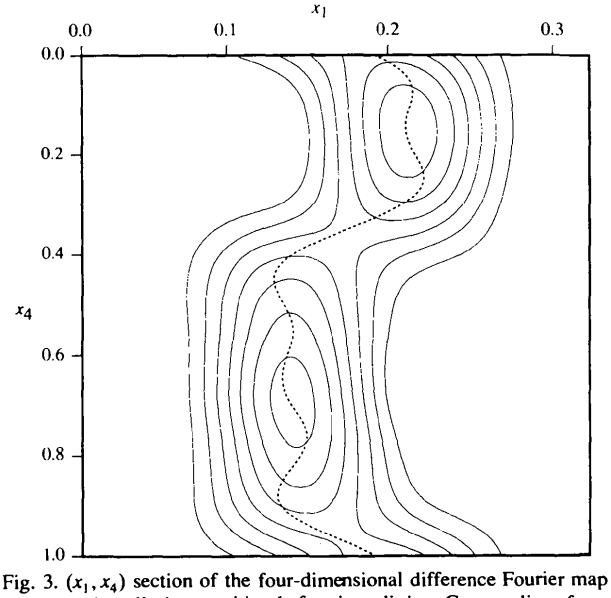

Fig. 3. (x_1, x_4) section of the four-dimensional difference Fourier map around the tellurium position before its splitting. Contour lines from 50 to 350 e Å^{-3} in intervals of 50 e Å^{-3}. The Te displacive modulation wave is shown as a broken line.

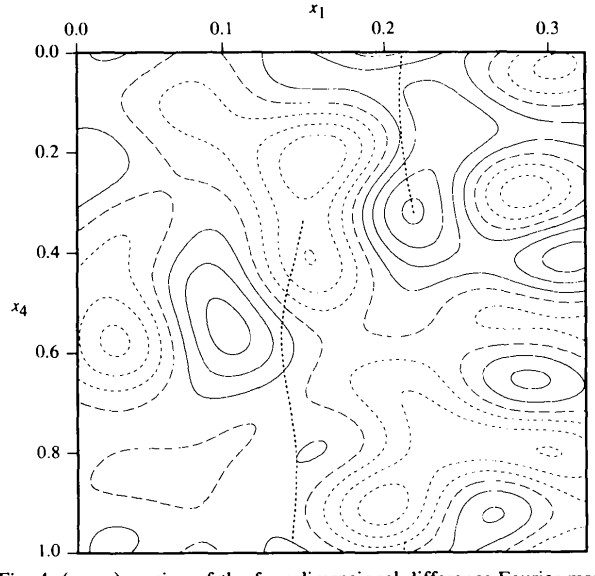

Fig. 4. (x_1, x_4) section of the four-dimensional difference Fourier map around the tellurium position after its splitting. Contour lines from −3 to 4 e Å^{-3} in intervals of 1 e Å^{-3} (positive and negative values in solid and broken lines, respectively). The Te displacive modulation wave is shown as a broken line.

Table 5. *Final values for the atomic displacement parameters*

$$U_{eq} = (1/3)\sum_i \sum_j U_{ij} a_i^* a_j^* \mathbf{a}_i . \mathbf{a}_j .$$

	$U_{eq(iso^*)}$	U_{11}	U_{22}	U_{33}	U_{12}	U_{13}	U_{23}
Ta(1)	0.0053 (2)	0.0062 (4)	0.0067 (3)	0.0030 (4)	0	0.0000 (3)	0
Ta(2)	0.0041 (3)	0.0035 (5)	0.0053 (4)	0.0034 (5)	0	−0.0001 (5)	0
Ge	0.0077 (7)						
Te(1)	0.0067 (2)	0.0060 (4)	0.0075 (4)	0.0066 (4)	−0.0006 (4)	−0.0011 (4)	0.0003 (4)
Te(2)	0.0063 (3)	0.0063 (6)	0.0069 (6)	0.0057 (5)	0.0005 (6)	0.0018 (5)	−0.0009 (6)

The expression of the displacement factor is: $\exp(-2\pi^2 \sum_i \sum_j U_{ij} a_i^* a_j^* \mathbf{h}_i \mathbf{h}_j)$, with U_{ij} in Å^2.

3. Discussion

Like most MA_xTe_2 structures, the $TaGe_{0.354}Te_2$ structure is built up from a close stacking of [Te,Te] sandwiches in an orthorhombic *AA/BB* mode. The van der Waals gap between successive trigonal prismatic sandwiches is empty. As already mentioned, the Ta and Ge atoms reside in the trigonal prismatic and square-planar coordination sites, respectively (see Fig. 5). Within an infinite sandwich plane, three different subunits built up from tellurium biprisms can be distinguished: the **a** ribbon with biprisms occupied by Ta–Ta pairs (*M2* biprism) and Ge atoms (*A* biprism), with the Ta–Ta pairs oriented at 150°, the **b** ribbon, similar to **a**, but with the Ta–Ta pairs at 30°, and finally the **c** ribbon with biprisms occupied with a lone Ta atom (*M* biprism). The sequence, within the sandwich, of the **a**, **b** and **c** rows is fully determined by the modulation wavelength (van der Lee, Evain, Monconduit, Brec, Rouxel & Petříček, 1994). Since $\frac{1}{3} \leq \gamma \leq \frac{2}{5}$, one expects the $TaGe_{0.354}Te_2$ slabs to be a succession of $TaGe_{1/3}Te_2$ and $TaGe_{2/5}Te_2$ basic entities (see Fig. 5), and with $\gamma = 0.3544$ (3) closer to $\frac{1}{3}$ than to $\frac{2}{5}$, one anticipates more $TaGe_{1/3}Te_2$ units than $TaGe_{2/5}Te_2$. Indeed, the plot of a fraction of the $TaGe_{0.354}Te_2$ slab (near the global phase origin) presented in Fig. 6 shows only two $TaGe_{2/5}Te_2$ units against seven $TaGe_{1/3}Te_2$ units.

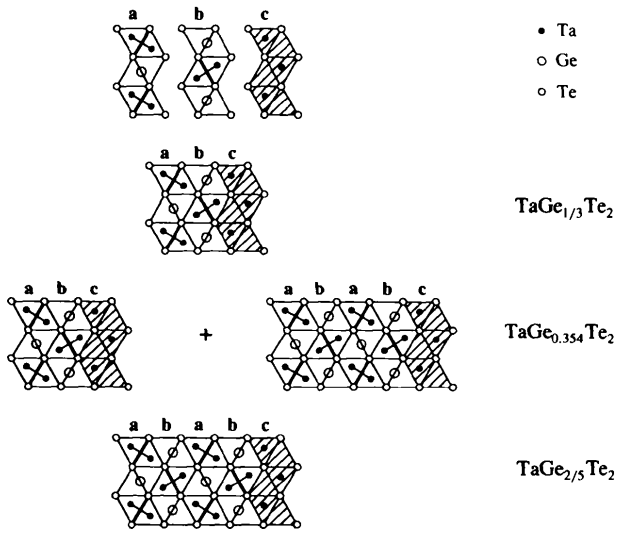

Fig. 5. The three ribbons **a**, **b** and **c** that are used to construct a $[TaGe_xTe_2]$ structural slab and the slab building for $x = \frac{1}{3}$, $x = \frac{2}{5}$ and $\frac{1}{3} < x < \frac{2}{5}$.

The validity of a structure determination is given not only by good reliability factors and a sensible geometry, but also by meaningful interatomic distances. This latter characteristic can be easily checked for a regular structure, either nonmodulated or commensurately modulated; however, it is less evident for an incommensurately modulated structure, especially with a strong occupation modulation. For instance, let us consider the in-plane Te—Te distances singled out (shaded) in Fig. 1 and referred as type I by Evain, van der Lee *et al.* (1994). Three different distances can be expected along the wavevector direction, one for each of the three different subunits: ~ 3.3 Å for the *M2* biprism, ~ 4.1 Å for the *A* biprism and finally ~ 3.6 Å for the *M* biprism (these three Te—Te distances will thereafter be referred to as Te—Te_{M2}, Te—Te_A and Te—Te_M, respectively). In the structure determination of $TaSi_{0.414}Te_2$, the type I Te—Te distances were obtained from a single modulated curve covering the three situations, that is with a broad dispersion (Fig. 7*a*). This modeling led to unrealistic

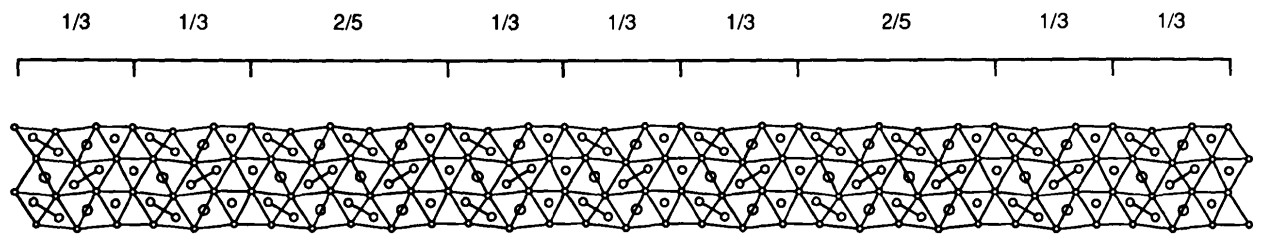

Fig. 6. *ORTEP* (Johnson, 1965) view of a fraction of the $TaGe_{0.354}Te_2$ slab (near the global phase origin) showing the succession of $TaGe_{1/3}Te_2$ and $TaGe_{2/5}Te_2$ building blocks.

Te—Te distances: too long for the longest, too short for the shortest and incorrect at the junction between the various situations. In the present structure determination, the use of proper crenel functions and the splitting of the Te position gave a more realistic set of distances, as can be seen in Fig. 7(*b*). The unique curve obtained for $TaSi_{0.414}Te_2$ splits into three domains, thereby approaching a crenel-like shape. The t domain limits and positions are simply related to the crenel widths and positions, respectively. This leads not only to valid distance ranges, but also to unbiased average distance values. The main features of such distance variations (d_{min}, d_{max} and $\langle d \rangle$) are gathered in Table 6.

Another test of the structure determination validity can be obtained through the analysis of the interslab interactions. Actually, it has recently been shown that this interaction in the MA_xTe_2 phases yields short through-the-gap Te···Te contacts, with or without a charge transfer at play (Evain, Monconduit & Brec, 1995). The short contacts are mainly due to the strong modulated distortion of the hexagonal Te sheets induced by the cation filling. In Fig. 8 the different unit interactions that can occur in the layer stacking ($M2/M2'$, A/A', $M2/A'$, A/M', M/M' and $M2/M'$) are presented. In these interactions, one particularly interesting contact has been singled out (shaded), corresponding to the type II Te···Te distance mentioned by Evain, van der Lee *et al.* (1994). This contact gives rise to the shortest Te···Te distance when it involves the stacking of two biprisms with Ta_2 pairs ($M2/M2'$, Fig. 8*a*). On the contrary, it generates the longest type II Te···Te distance across the van der Waals gap for two biprisms with Ge atoms (A/A', Fig. 8*b*). Other possibilities are illustrated in Figs. 8(*c*)–(*f*), leading to intermediate distances. Such differences in type II Te—Te distances are perfectly reproduced in the plot presented in Fig. 9. Indeed, four t intervals with different Te—Te distance ranges can be seen, corresponding to the situations illustrated in Figs. 8(*a*)–(*d*). For $0.0 < t < 0.1614$ and $0.8386 < t < 1.0$ (curve 1 in Fig. 9), the domains t_{M2} and $t_{M2'}$ overlap, indicating a stacking of two biprisms with Ta_2 pairs ($M2/M2'$, Fig. 8*a*). This configuration generates short Te···Te contact distances around 3.79 Å. For $0.4842 < t < 0.5158$, the situation with two Ge

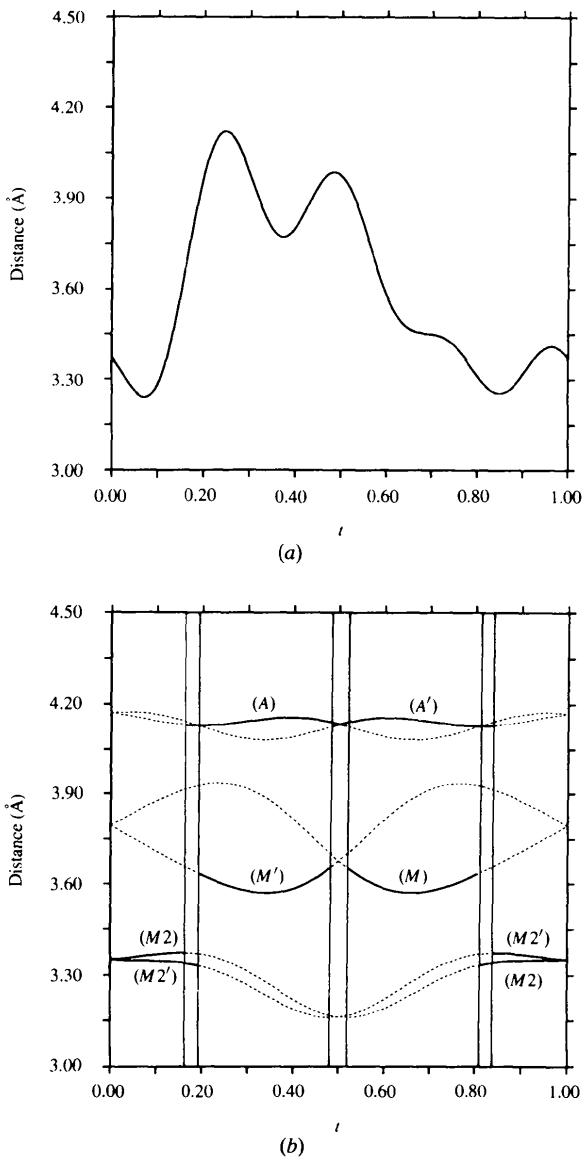

Fig. 7. Te—Te type I in-slab distances (Å) in (*a*) $TaSi_{0.414}Te_2$ and (*b*) $TaGe_{0.354}Te_2$. $M2$, A and M are units at $y = \frac{1}{4}$ and $M2'$, A' and M' are units at $y = \frac{3}{4}$.

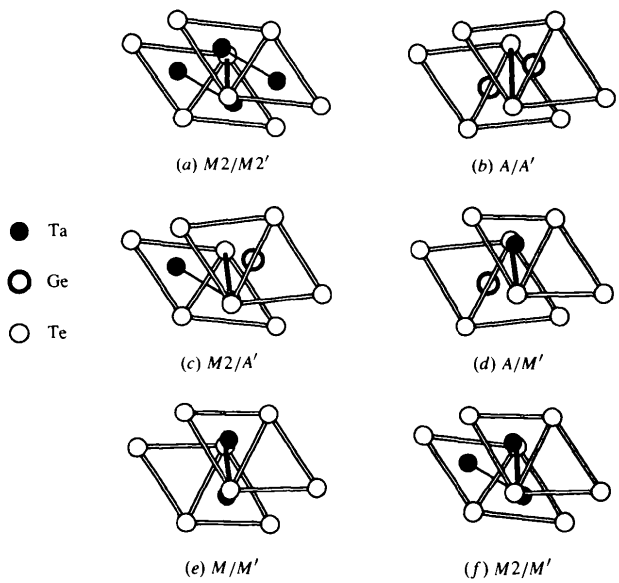

Fig. 8. The different possibilities of unit stacking in MA_xTe_2 structures. One particular inter-slab Te···Te contact (type II) is singled out.

Table 6. *Main interatomic distances (Å) in* $TaGe_{0.354}Te_2$

	$\langle d \rangle$	d_{min}	d_{max}		$\langle d \rangle$	d_{min}	d_{max}
Ta(1)—Te(1) (×2)	2.82	2.76	2.93	Ta(2)—Te(1) (×2)	2.95	2.92	2.99
Ta(1)—Te(1) (×2)	2.82	2.80	2.91	Ta(2)—Te(2) (×2)	2.83	2.81	2.85
Ta(1)—Te(2) (×2)	2.81	2.68	2.91	Ta(2)—Te(2) (×2)	2.82	2.79	2.83
Ta(1)—Te(2) (×2)	2.96	2.90	2.99				
				Ta(1)—Ta(2)	2.89	2.81	2.92
Ge—Te(1) (×2)	2.81	2.76	2.83				
Ge—Te(2) (×2)	2.76	2.72	2.82				
Ta(1)—Ge	2.86	2.80	2.89	Ta(2)—Ge	2.82	2.75	2.85
Ta(1)—Ge	2.75	2.69	2.86	Ta(2)—Ge	2.84	2.76	2.88
Te—Te distances parallel to the layer (Type I)				Te—Te distances through the van der Waals gap (Type II)			
Te(1)—Te(1) (*M*)	3.60	3.57	3.65	Te(1)—Te(1) (1)	3.79	3.72	3.85
Te(1)—Te(2) (*A*)	4.14	4.13	4.16	Te(1)—Te(2) (2,3)	3.97	3.96	4.00
Te(1)—Te(2) (M_2)	3.36	3.34	3.37	Te(2)—Te(2) (4)	4.25	4.25	4.25

atoms occurs (A/A', Fig. 8*b*), corresponding to the overlapping of the domains t_A and $t_{A'}$, and a long distance of ~ 4.25 Å is found. Notice that this case is quite rare in the structure since the corresponding t interval is small (3.16%). It can be shown that this percentage corresponds to the frequency of the Te(I—I) unit, $(3x-1)/2$, which is nil for $x = \frac{1}{3}$ and maximum ($\frac{1}{4}$) for $x = \frac{1}{2}$. The other two situations, $0.1614 < t < 0.1930$ ($0.8070 < t < 0.8386$) and $0.1930 < t < 0.4842$ ($0.4148 < t < 0.8070$) corresponding to $A/M2'$ ($A'/M2$) (Fig. 8*c*) or A/M' ($A'M$) (Fig. 8*d*) interactions, respectively, are found in the same curves (2 and 3 of Fig. 9). It is worth noting that the stackings of two biprisms with lone metals (M/M', Fig. 8*e*) or of two biprisms with a metal pair in one and a lone metal in the other ($M2/M'$, Fig. 8*f*) are never found in the structure (and as a matter of fact never found in any commensurate MA_xTe_2 phases). These situations never occur because the corresponding crenel functions do not overlap (see Fig. 9).

Although this is the first MA_xTe_2 phase found in the Ta–Ge–Te system and, therefore, no simple comparisons with homologous structures can be made, it is nevertheless possible to review some main structural features. First, the average Ta—Ta distance of the Ta_2 pair (2.89 Å) compares very well with the distance calculated in $TaSi_{1/3}Te_2$ (2.902 Å). Secondly, as expected, the Ta—Ge distances are found to be a little longer (2.69–2.89 Å) than the Ta—Si distances in $TaSi_{1/3}Te_2$ (2.70–2.82 Å), in agreement with the larger cation size of Ge^{2+}. Finally, the square-planar-like environment of Ge seems to be a constant of the MGe_xTe_2 phases, with $d_{Ge-Te} = 2.72$–2.83 Å in $TaGe_{0.354}Te_2$ and $d_{Ge-Te} = 2.74$–2.79 Å in $TaGe_{1/3}Te_2$.

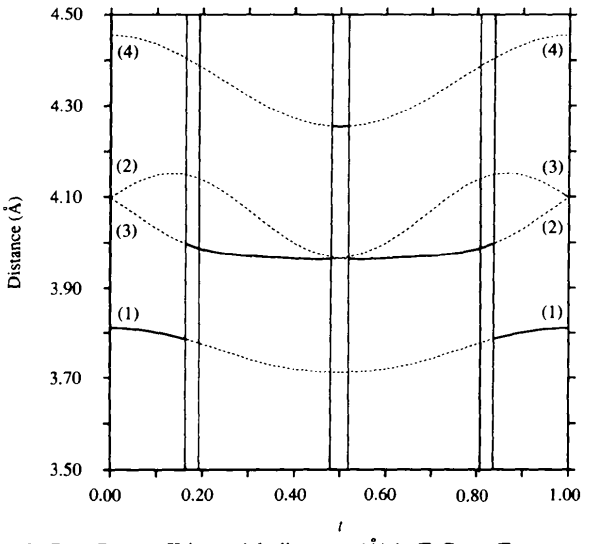

Fig. 9. Te—Te type II inter-slab distances (Å) in $TaGe_{0.354}Te_2$.

4. Concluding remarks

We have clearly shown that the use of crenel functions, in combination with an orthogonalization of the associated displacive modulation functions, can greatly improve the accuracy of a structure determination of a phase with strong occupation modulation waves. Crenel functions can be used in describing the occupation, not only of the atoms with a partial occupancy, but also of other atoms (with a full occupancy) which are bound to be heavily displaced from their average positions. Such a procedure prevents the calculation of unreliable distances that would otherwise necessarily occur because of a lack of piecewise constant displacive modulation functions in the refinement. In some ways, the structure proves as easy to interpret as a normal commensurate structure would be.

The research of VP has been made possible by the grant 202/93/1154 from the Grant Agency of the Czech Republic.

References

Böttcher, P. (1988). *Angew. Chem.* **100**, 781–794.
Canadell, E., Jobic, S., Brec, R., Rouxel, J. & Whangbo, M.-H. (1992). *J. Solid State Chem.* **99**, 189–199.
Canadell, E., Monconduit, L., Evain, M., Brec, R., Rouxel, J. & Whangbo, M.-H. (1993). *Inorg. Chem.* **32**, 10–12.
Enraf–Nonius (1989). *CAD-4 Software*. Enraf–Nonius, Delft, The Netherlands.

Evain, M. (1992). *U-FIT* Program. I.M.N. Internal Report, Nantes, France.

Evain, M., van der Lee, A., Monconduit, L. & Petříček, V. (1994). *Chem. Mater.* **6**, 1776–1783.

Evain, M., Monconduit, L. & Brec, R. (1995). *J. Solid State Chem.* In the press.

Evain, M., Monconduit, L. & van der Lee, A. (1995). In preparation.

Evain, M., Monconduit, L., van der Lee, A., Brec, R., Rouxel, J. & Canadell, E. (1994). *New J. Chem.* **18**, 215–222.

Gareh, J., Boucher, F. & Evain, M. (1995). *Eur. J. Solid Inorg. Chem.* Submitted.

Hall, S. R., Flack, H. D. & Stewart, J. M. (1992). Editors. *Xtal*3.2 *Reference Manual.* Universities of Western Australia, Australia, Geneva, Switzerland, and Maryland, USA.

Jobic, S., Brec, R. & Rouxel, J. (1992). *J. Alloys Compd*, **178**, 253–283.

Johnson, C. K. (1965). *ORTEP.* Report ORNL-3794. Oak Ridge National Laboratory, Tennessee, USA.

Lee, A. van der & Evain, M. (1995). *Aperiodic '94, Conference Proceedings*, edited by G. Chapius & W. Paciorek, p. 440. Singapore: World Scientific Publishing.

Lee, A. van der, Evain, M., Mansuetto, M., Monconduit, L., Brec, R. & Rouxel, J. (1994). *J. Solid State Chem.* **111**, 75–82.

Lee, A. van der, Evain, M., Monconduit, L., Brec, R., Rouxel, J. & Petříček, V. (1994). *Acta Cryst.* B**50**, 119–128.

Lee, A. van der, Evain, M., Monconduit, L., Brec, R. & van Smaalen, S. (1994). *J. Phys. Condens. Matter*, **6**, 933–944.

Li, J. & Caroll, P. J. (1992). *Mater. Res. Bull.* **27**, 1073–1081.

Li, J., Badding, E. & DiSalvo, F. J. (1992). *J. Alloys Compd*, **184**, 257–263.

Mar, A., Jobic, S. & Ibers, J. A. (1992). *J. Am. Chem. Soc.* **114**, 8963–8971.

Monconduit, L., Evain, M., Boucher, F., Brec, R. & Rouxel, J. (1992). *Z. Anorg. Allg. Chem.* **616**, 177–182.

Monconduit, L., Evain, M., Brec, R., Rouxel, J. & Canadell, E. (1993). *C. R. Acad. Sci. Paris*, **314**, 25–34.

Petříček, V. (1994). *JANA*94. *Programs for Modulated and Composite Crystals.* Institute of Physics, Praha, Czech Republic.

Petříček, V., van der Lee, A. & Evain, M. (1995). *Acta Cryst.* A**51**, 529–535.

Rouxel, J. (1993). *Comm. Inorg. Chem.* **14**, 207–228.